Journal of Alloys and Compounds 505 (2010) 584–587

Contents lists available at ScienceDirect

Journal of Alloys and Compounds

journal homepage: www.elsevier.com/locate/jallcom

Crystal interstitial sites contribution to nitrogen supersaturation in mechanically alloyed Fe–Cr–Mn–N alloys

E. Salahinejad [a,*], R. Amini [a,b], M. Ghaffari [c], M.J. Hadianfard [a]

[a] Department of Materials Science and Engineering, School of Engineering, Shiraz University, Zand Blvd., 7134851154, Shiraz, Iran
[b] Department of Materials Science and Engineering, Shiraz University of Technology, Modarres Blvd., 3619995161, Shiraz, Iran
[c] School of electrical electronic engineering, Nanyang technological University, Nanyang avenue, Singapore 639798, Singapore

ARTICLE INFO

Article history:
Received 12 April 2010
Received in revised form 9 June 2010
Accepted 11 June 2010
Available online 23 June 2010

Keywords:
Mechanical alloying
Nanostructured materials
Amorphous materials
X-ray diffraction
Microstructure
Interstitial alloys

ABSTRACT

In the recent years, the addition of nitrogen to iron alloys by mechanical alloying has attracted considerable attention. In this paper, mechanical alloying of Fe–18Cr–8Mn powder mixture under a nitrogen atmosphere is considered from the viewpoints of nitrogen supersaturation and phase transformation. By progression of milling, austenitization and amorphization transformations are detected. The contribution of interstitial sites of the nanocrystalline phases to the nitrogen supersaturation is estimated by X-ray diffraction experiments. It is found that the contribution is progressively decreased by increasing the total nitrogen content. Typically, only about 4% of total incorporated nitrogen is distributed among the crystal interstitial sites of the Fe–18Cr–8Mn–2.5N alloy.

1. Introduction

Cr–Mn–N stainless steels have attracted much attention from scientific and technological points of view in the recent years. It is well established that the nitrogen addition to stainless steels has advantageous effects on their mechanical properties [1–5] and corrosion resistance [5–7]. Nitrogen in stainless steels is strong austenite stabilizer and biocompatible; therefore, it is capable of being a replacement for nickel which is expensive and toxic. Despite the fact that the effect of dissolved nitrogen on the austenite stabilization is several times higher than that of nickel, the nitrogen solubility is limited due to nitride formation. To increase the nitrogen solubility, manganese is an appropriate alloying element that is generally used along with nitrogen in nickel-free stainless steels [8].

It has been found that the nitrogen solubility in the liquid state is limited and complex melting processes with a nitrogen overpressure are required to produce high-nitrogen alloys [8–10]. Currently, mechanical alloying (MA) has been regarded as an alternative solid-state route to synthesize these alloys. Nitrogen alloying via MA can be accomplished by either milling under a nitrogen atmosphere or milling with proper nitrides under an inert gas. The generation of the high density of defects during MA increases the nitrogen solubility considerably [11–19]. In the recent years, noticeable researches on MA of Ni-free stainless steels under a nitrogen atmosphere have been also reported [11–19].

Concerning the nitrogen distribution in the structure of nitrogen-containing steels, no significant nitrogen segregation at grain boundaries has been found in nitrogen-containing ferritic steels [20]. Moreover, Petrov et al. [21] have reported that nitrogen atoms have no detectable affinity to grain boundaries of high-alloyed austenitic steels. The nitrogen distribution in Fe-based alloys synthesized by MA under a nitrogen atmosphere has been tacitly analyzed [11,13,22–24]. Most of them have attributed the nitrogen supersaturation to preferential sites at dislocation elastic stress fields and nanograin boundaries developed during MA. Typically, Rawers et al. [24,25] have shown that in Fe–4.1N and Fe–1.36N alloys prepared by MA, 50% and 25% of nitrogen are entrapped into the crystal interstitial sites, respectively. To our knowledge, no systematic work has been reported on the contribution of the crystal interstitial sites to the nitrogen supersaturation of stainless steels. This study evaluates the supersaturation and distribution of nitrogen among crystal interstitial sites of mechanically alloyed nanocrystalline/amorphous 18Cr–8Mn–*x*N stainless steel powders.

2. Experimental procedures

MA of pure elemental Fe (>99.5%, $D_{av.}$ = 50 μm), Cr (>99.9%, $D_{av.}$ = 150 μm), and Mn (>99.9%, $D_{av.}$ = 50 μm) powders supplied by Merck, with the weight ratio of 74:18:8, was performed in a high-energy shaker mill. Prior to processing, the grind-

* Corresponding author. Tel.: +98 917 3879390; fax: +98 711 230 7293.
E-mail address: erfan.salahinejad@gmail.com (E. Salahinejad).

0925-8388/$ – see front matter © 2010 Elsevier B.V. All rights reserved.
doi:10.1016/j.jallcom.2010.06.079

Table 1
Chemical composition of the Fe–18Cr–8Mn powders milled under nitrogen (wt.%).

Milling time (h)	Fe	Cr	Mn	N	O	C
24	72.978	17.748	8.225	0.693	0.325	0.032
48	72.948	17.643	8.069	0.973	0.334	0.033
72	72.971	17.505	7.827	1.330	0.334	0.033
96	72.763	17.408	7.705	1.760	0.335	0.029
120	72.530	17.350	7.629	2.130	0.331	0.030
144	72.319	17.203	7.576	2.537	0.334	0.031

ing vessel was flushed several times with nitrogen gas. Milling was accomplished under a continuous flow (10 mL/min) of high-purity nitrogen gas and argon gas at a rotation speed of 400 rpm. A ball-to-powder weight ratio of 10:1 was employed by a combination of two different sizes of hardened steel balls (4×20 mm and 7×8 mm). Powder sampling was performed at 24-h intervals, ranging from 24 to 144 h, inside a nitrogen glove box.

The chemical composition of the milled powders was determined by a LECO gas analyzer (Corp., St. Joseph, MI) and X-ray fluorescence analyzer (XRF, Philips PW2400). X-ray diffraction (XRD) experiments were conducted on the powders by Shimadzu Lab X-6000 with Cu Kα radiation. The quantitative analysis of the XRD data was carried out by TOPAS 3 from Bruker AXS. By this software, the relative content of present phases was estimated by the Rietveld method and the average crystallite size of the crystalline phases was determined by the Double-Voigt approach. The amorphous phase content was also determined by Rietveld analyzing the XRD pattern of a mixture of the as-milled powders and the known amount of nanocrystalline Fe powder as a standard, as detailed in Ref. [14]. The validity of the XRD results was checked by transmission electron microscopy (TEM, JEOL-JEM 2010). The amount of nitrogen distributed among the crystal interstitial sites was estimated via changes in lattice plane spacing determined by the XRD analyses.

3. Results and discussion

3.1. Structural evolution during MA

The results of the elemental analyses on the powders milled under nitrogen gas are listed in Table 1. It is seen that the total nitrogen amount progressively increases from 0.7 to 2.5 wt.%, when the milling time increases from 24 to 144 h, whereas the oxygen content is remained constant. The detected oxygen is due to the natural oxidation of the powders in the atmosphere. In the case of milling under nitrogen gas, molecular nitrogen adheres on virgin surfaces created during MA, dissociates, and consequently penetrates into the matrix via cold welding of the particles and diffusing down to interstitial sites, grain boundaries, dislocations, and other defects.

It is known that the equilibrium solubility limit of nitrogen in iron at room temperature is less than 0.1 wt.% [11,19]. The addition of alloying elements like Cr and Mn that are located in the left of Fe in the periodic table enhances the nitrogen solubility. However, this fact cannot alone justify the observed nitrogen supersaturation. During milling, the high amount of structural defects like point defects, dislocations, and nanograin boundaries is generated due to severe plastic deformation [26]. Since the mismatch strain of solute nitrogen is reduced in the defects, a high proportion of nitrogen atoms are diffused down to the defects. Mossbauer studies of high-nitrogen iron powders prepared by MA have signified that a considerable amount of infused nitrogen accumulates at grain boundaries [24,25].

The XRD analyses were conducted on the as-milled powders; the related XRD traces are available in Ref. [14]. According to the Rietveld analysis, three different phases, namely ferrite (α), austenite (γ), an amorphous phase, are recognizable. Table 2 summarizes the results of the XRD analyses, consisting of the relative phase amounts and the crystallites sizes. It is seen that in the short milling durations, the amount of the α-phase is more than that of the γ-phase; however, by progression of milling, the austenitization transformation progresses, leading to the domination of the γ-phase to the α-phase in the long milling durations. In addition, the amorphous phase content is considerable, reaching about 84 wt.% after 144 h of milling. Fig. 1 shows the TEM micrograph of the powder milled for 48 h having a nanocomposite structure. The selected area diffraction (SAD) patterns imply that the dark regions are a combination of the nanocrystalline α- and γ-phases and the bright matrix is a featureless amorphous phase. That is, the TEM assessments confirm what the XRD analyses show [14].

Table 2
Results of the XRD experiments on the Fe–18Cr–8Mn powders milled under nitrogen.

Milling time (h)	α-phase percentage	γ-phase percentage	Amorphous percentage	α-crystallite size (nm)	γ-crystallite size (nm)
24	51.7	19.3	29.0	18	16.2
48	22.9	37.8	39.3	15.2	14.2
72	17.7	38.6	43.7	11.7	11.3
96	11.7	33.9	54.4	9.8	8.2
120	5.3	27.3	67.4	7.8	6.1
144	1.4	14.9	83.7	6.3	5.2

The powder particles are subjected to severe plastic deformation during MA; thus, the density of dislocations increases and shear bands containing high dislocation densities develop. To decrease lattice strain, dislocation cells and subgrains separated by low-angle grain boundaries are formed. Finally, the transformation of the low-angle to high-angle grain boundaries occurs by grain rotation, giving nanostructures [26]. Moreover, it has been also realized that the nitrogen incorporation during MA intensifies the grain refinement [14]. Diffused nitrogen atoms are segregated at dislocations and grain boundaries, fixing the dislocations and stabilizing the grain boundaries. Afterward, the trickling down of mobile dislocations on the fixed dislocations contributes to the nucleation of new boundaries and accordingly severe grain refinement [14,27].

As it is obvious in Table 2, by progression of MA, the ferrite-to-austenite transformation proceeds. Nitrogen atoms diffuse into interstitial sites of the ferrite crystallites and produce mismatch strains. Since austenite has larger interstitial sites than ferrite, nitrogen atoms in austenite create less distortion and volume mismatch. In addition, austenite has smaller interfacial energy compared with ferrite [14]. As well as these effects, the structural refinement to the nanometric scale favors the austenitization transition during MA [13,19]. The grain refinement leads to an increase in the volume fraction of interfaces (grain boundaries); typically, the density of grain boundaries reaches 10^{19} cm^{-3} [28]. In this case, the enthalpy or strain energy of the material is such high as high-temperature phase transformations like austenitization are promoted at room temperature [29,30]. The final decreasing trend

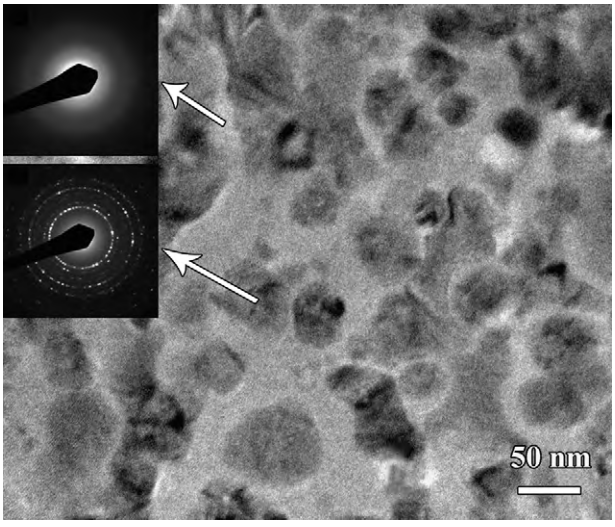

Fig. 1. TEM micrograph of the powder milled for 48 h under nitrogen. The insets indicate the SAD pattern of the different regions.

Table 3
Values of a_{α}^{Ar}, a_{α}^{N}, a_{γ}^{N}, $[N_{\alpha}]$, $[N_{\gamma}]$, N_{int}, and N_{int}%.

Milling time (h)	a_{α}^{Ar} (Å)	a_{α}^{N} (Å)	a_{γ}^{N} (Å)	$[N_{\alpha}]$ (wt.%)	$[N_{\gamma}]$ (wt.%)	N_{int} (wt.%)	N_{int}%
24	2.8654	2.8759	3.5987	0.387	0.306	0.259	37.374
48	2.8657	2.8792	3.6048	0.497	0.480	0.295	30.319
72	2.8661	2.8838	3.6083	0.652	0.580	0.339	25.489
96	2.8663	2.8885	3.6098	0.818	0.623	0.307	17.443
120	2.8665	2.8893	3.6113	0.840	0.666	0.226	10.610
144	2.8868	2.8906	3.6138	0.140	0.737	0.112	4.415

in the austenite content is owing to the amorphization of the austenite nanostructures, when the amorphization prevails over the ferrite-to-austenite transformation as the dissolved nitrogen approaches the considerable values.

The amorphization reaction can be argued by the high energy given to the powders during milling and the influence of nitrogen. The extreme structural refinement that has occurred during milling increases the constraint of the neighboring crystallites, decreasing the stability of the crystalline structure. Moreover, nitrogen intensifies the structural refinement, aiding amorphization. On the other hand, nitrogen in the Fe–Cr–Mn–N alloys increases the atomic size mismatch and negative heat of mixing among the constituent elements [14–18], encouraging amorphization significantly according to the Inoue's empirical rules [31].

3.2. Estimation of interstitial nitrogen content in the nanocrystals

In general, the nitrogen infusion into materials can be accompanied with (i) the precipitation of nitrides, (ii) the dissolution into interstitial sites of crystallites, (iii) the segregation at defects like grain boundaries and dislocations, and (iv) the distribution among interstitial sites of the amorphous phase. Regarding the contribution of nitrides to the nitrogen incorporation, no nitride precipitate was detected in the milled powders, according to the Rietveld analysis of the XRD results by the TOPAS software. It is noted that all probable nitride compounds were considered in the Rietveld analyses. Albeit, it should be considered that very low nitride contents cannot be detected by the XRD method.

The interstitial nitrogen dissolution within ferrite and austenite crystals distorts the host crystal lattice, leading to changes in interplane spacing. In the case of milling under an inert argon atmosphere, instead of nitrogen, no such change in lattice interplane spacing is detected [11,23]. Accordingly, from the shift of (1 1 0) peak of the α-phase in the XRD patterns, the content of nitrogen dissolved interstitially in this phase can be estimated. Note that nitrogen atoms occupy the octahedral interstitial sites in the crystalline phases like carbon atoms. Wriedt et al. [32] have pointed out an empirical equation (Eq. (1)) to relate the dissolved nitrogen content in the α-phase ($[N_{\alpha}]$) to the interplanar spacing ($d_{(1\,1\,0)}$).

$$[N_{\alpha}](\text{wt.\%}) = 52.0833(d_{(1\,1\,0)}(\text{Å}) - 2.0268) \quad (1)$$

where the constant 2.0268 is the (1 1 0) interplanar spacing of nitrogen-free samples. However, the equation does not take account of the influences of alloying element and milling process. Rawers et al. [23] have found that this constant should be modified to 2.029 to be applicable to mechanically alloyed Fe–N alloys having a heavily deformed nanostructure. In this study, to have accurate estimations for the mechanically alloyed Fe–Cr–Mn–N alloys, the constant is calculated from the XRD analysis of the powders milled under argon. Indeed, this procedure considers the effects of the alloying elements (Cr and Mn) and the milling process on the interplanar spacing. On the other hand, since the amount of the other interstitial elements, i.e. oxygen and carbon, in the samples milled under both the atmospheres was the same, their role in the evolution of the interplanar spacing is separated by this method. Converting the (1 1 0) interplanar spacing to the lattice parameter yields the following equation:

$$[N_{\alpha}](\text{wt.\%}) = 36.8285(a_{\alpha}^{N}(\text{Å}) - a_{\alpha}^{Ar}(\text{Å})) \quad (2)$$

where a_{α}^{N} and a_{α}^{Ar} are the lattice parameter of the α-phase in the powders milled under the nitrogen and argon atmospheres, respectively.

On the other hand, Danilkin et al. [33] have suggested another empirical equation (Eq. (3)) to relate the interstitial nitrogen concentration of the austenite phase ($[N_{\gamma}]$) to the lattice parameter a_{γ}^{N}.

$$[N_{\gamma}](\text{wt.\%}) = 28.5714(a_{\gamma}(\text{Å}) - 3.588) \quad (3)$$

Since austenitization does not occur in the powders milled under argon, it was not possible to calculate the austenite lattice parameter in the N-free samples. The lattice parameter of the α- and γ-phases after the Rietveld refinement of the XRD data and also the dissolved nitrogen contents calculated from Eqs. (2) and (3) are listed in Table 3. Using the relative content of the α- and γ-phases presented in Table 2 and considering the linear combination of these two phases in the interstitial nitrogen distribution, the average dissolved nitrogen content in the crystal interstitial sites (N_{int}) is also tabulated in Table 3, i.e. $N_{int} = \{(\alpha\%)(N_{\alpha}) + (\gamma\%)(N_{\gamma})\}/100$.

Table 3 reflects that N_{int} first increases and then decreases by progression of milling from 24 to 144 h. In the short milling durations up to 72 h, the crystalline phases are dominant and nitrogen atoms are occupying the interstitial sites, which finally leads to the nitrogen saturation. This is due to the fact that the nitrogen solubility in the crystalline phases is limited. In addition, in this period the progression of the α-to-γ phase transformation provides the larger crystal interstitial sites, giving rise to the increase in N_{int}. However, in the long milling durations, nitrogen saturation in the crystal interstitial sites has occurred and amorphization prevails. Since the defect density reaches considerable values and the amorphous phase is dominated, nitrogen atoms prefer to go to the defects (particularly nanograin boundaries and dislocation cores) and the amorphous phase to decrease the strain energy. Dividing the amounts of crystal interstitial nitrogen by those of total infused nitrogen (N_{int}%) demonstrates that, the contribution of the interstitial sites to the nitrogen supersaturation progressively decreases by increasing the milling time. 37–4% of the total infused nitrogen is entrapped into the crystal interstitial sites for the milling durations of 24–144 h. Hence, it is straightforwardly inferred that the considerable amount of nitrogen is distributed among the other sites of the structure consisting of the defects and amorphous phase. Compared to other researches [24,25], the minor contribution of the crystal interstitial sites to the supersaturation in this work is attributed to the development of the considerable contents of the amorphous phase providing more preferential sites for nitrogen atoms. Note that the amorphization reaction in the Fe–Cr–Mn–N system is more active than the Fe–N system studied in Refs. [24,25]. Eventually, it is noted that aspects of sintering and mechanical behaviors of these mechanically alloyed Cr–Mn–N stainless steels have been recently focused [34–37].

4. Conclusions

In this paper, MA of Fe–18Cr–8Mn powder mixture under nitrogen was investigated in terms of the nitrogen supersaturation, nanocrystallization, ferrite-to-austenite phase transformation, and amorphization. The contribution of the crystal interstitial sites to the nitrogen supersaturation was estimated quantitatively via XRD analyses from the evolution of interplane spacing with the milling time. It was found that the contribution of the interstitial sites to the total supersaturation decreases by progression of MA. Typically, only 4% of the total infused nitrogen was entrapped into the crystal interstitial sites of the sample milled for 144 h. By progression of milling, nitrogen atoms prefer to go to the defects and amorphous phase to decrease the strain energy. Accordingly, the major contribution to the nitrogen supersaturation was attributed to the elastic stress field of dislocations, nanograin boundaries, and amorphous phase developed by MA.

References

[1] J. Rawers, M. Grujicic, Mater. Sci. Eng. A 207 (1996) 188–194.
[2] D.W. Kim, W.S. Ryu, J.H. Hong, S.K. Choi, J. Nucl. Mater. 254 (1998) 226–233.
[3] J.B. Vogt, J. Mater. Process. Technol. 117 (2001) 364–369.
[4] J. Freudenberger, A. Gaganov, A.L. Hickman, H. Jones, Cryogenics 43 (2003) 133–136.
[5] J.W. Simmons, Mater. Sci. Eng. A 207 (1996) 159–169.
[6] I. Olefjord, L. Wegrelius, Corros. Sci. 38 (1996) 1203–1220.
[7] H. Baba, T. Kodama, Y. Katada, Corros. Sci. 44 (2002) 2393–2407.
[8] M. Sumita, T. Hanawa, S.H. Teoh, Mater. Sci. Eng. C 24 (2004) 753–760.
[9] G. Balachandran, M.L. Bhatia, N.B. Ballal, P.K. Rao, ISIJ Int. 41 (2001) 1018–1027.
[10] N. Nakada, N. Hirakawa, T. Tsuchiyama, S. Takaki, Scripta Mater. 57 (2007) 153–156.
[11] M.M. Cisneros, H.F. Lopez, H. Mancha, D. Vazquez, E. Valdes, G. Mendoza, M. Mendez, Metall. Mater. Trans. A 33 (2002) 2139–2144.
[12] M. Mendez, H. Mancha, M.M. Cisneros, G. Mendoza, J.I. Escalante, H.F. Lopez, Metall. Mater. Trans. A 33 (2002) 3273–3278.
[13] M.M. Cisneros, H.F. Lopez, H. Mancha, E. Rincon, D. Vazquez, M.J. Perez, S.D.D.L. Torre, Metall. Mater. Trans. A 36 (2005) 1309–1316.
[14] R. Amini, M.J. Hadianfard, E. Salahinejad, M. Marasi, T. Sritharan, J. Mater. Sci. 44 (2009) 136–148.
[15] R. Amini, H. Shokrollahi, E. Salahinejad, M.J. Hadianfard, M. Marasi, T. Sritharan, J. Alloys Compd. 480 (2009) 617–624.
[16] E. Salahinejad, R. Amini, M. Marasi, T. Sritharan, M.J. Hadianfard, Mater. Chem. Phys. 118 (2009) 71–75.
[17] R. Amini, E. Salahinejad, M.J. Hadianfard, M. Marasi, T. Sritharan, Mater. Sci. Eng. A 527 (2010) 1135–1142.
[18] E. Salahinejad, R. Amini, E. Askari Bajestani, M.J. Hadianfard, J. Alloys Compd. 497 (2010) 369–372.
[19] T. Haghir, M.H. Abbasi, M.A. Golozar, M. Panjepour, Mater. Sci. Eng. A 507 (2009) 144–148.
[20] M.L. Rudy, R.A. Huggins, TMS AIME 236 (1966) 1662–1666.
[21] Y.N. Petrov, V.G. Gavriljuk, H. Berns, Ch. Escher, Scripta Mater. 40 (1999) 669–674.
[22] C.J. Rawers, R.C. Doan, Metall. Mater. Trans. A 25 (1994) 381–388.
[23] C.J. Rawers, D. Maurice, Acta Mater. 43 (1995) 4101–4107.
[24] C.J. Rawers, D. Govier, R. Doan, Mater. Sci. Eng. A 22 (1996) 162–167.
[25] J.C. Rawers, R. Krabbe, D.C. Cook, T.H. Kim, Nanostruct. Mater. 9 (1997) 145–148.
[26] C. Suryanarayana, Prog. Mater. Sci. 46 (2001) 1–184.
[27] E.P. Yelsukov, G.A. Dorofeev, A.V. Zagainov, N.F. Vildanova, A.N. Maratkanova, Mater. Sci. Eng. A 369 (2004) 16–22.
[28] J.C. De Lima, V.H.F. Dos Santos, T.A. Grandi, P.C.T. D'Ajello, A. Dmitriev, Phys. Rev. B 62 (2000) 8871–8877.
[29] H.J. Fecht, Acta Metall. Mater. 38 (1990) 1927–1932.
[30] Q. Meng, N. Zhou, Acta Mater. 50 (2002) 4563–4570.
[31] A. Inoue, T. Zhang, T. Masumoto, J. Non-Cryst. Solids 156–158 (1993) 473–480.
[32] H.A. Wriedt, N.A. Gokcen, R.H. Nafziger, Bull. Alloy Phase Diagr. 8 (1987) 355–377.
[33] S. Danilkin, A. Beskrovni, E. Jadrowski, Mater. Sci. Forum 318–320 (1999) 19–24.
[34] E. Salahinejad, R. Amini, M. Ghaffari, M.J. Hadianfard, Mater. Sci. Eng. A 527 (2010) 5522–5527.
[35] E. Salahinejad, R. Amini, M. Marasi, M.J. Hadianfard, Mater. Des. 31 (2010) 527–532.
[36] E. Salahinejad, R. Amini, M. Marasi, M.J. Hadianfard, Mater. Des. 31 (2010) 2259–2263.
[37] E. Salahinejad, R. Amini, M.J. Hadianfard, Mater. Des. 31 (2010) 2241–2244.